

Classical Simulation of Ultracold Dipolar Collisions

by

Alex Adler

A thesis submitted to the Faculty of the
University of Colorado in partial fulfillment
of the requirements for the award of

Departmental Honors

Department of Physics

2022

This thesis entitled:
Classical Simulation of Ultracold Dipolar Collisions
written by Alex Adler
has been approved for the Department of Physics

John L. Bohn (Physics)

Jun Ye (Physics)

Peter Mayr (Mathematics)

Date: 29 March 2022

The final copy of this thesis has been examined by the signatories, and we find that both the content and the form meet acceptable presentation standards of scholarly work in the above mentioned discipline.

Adler, Alex (University of Colorado at Boulder)

Classical Simulation of Ultracold Dipolar Collisions

Thesis directed by Prof. John L. Bohn (Physics)

Most physicists' intuitions are classically driven, for our lived experience takes place entirely in the classical limit. Even in situations which are completely quantum mechanical in nature, starting with a classical calculation helps us understand generally how systems work and where we should look to manipulate them. In this thesis, a classical simulation is used to predict the likelihood and orientation of a collision between two KRb molecules for various initial conditions and external field strengths. The simulation uses the classical Hamiltonian for two dipoles in an external field to numerically solve for the position, internal angles, momentum, and angular momentum of each molecule. Three general cases are considered: free dipoles in zero external electric field, dipoles in a large field that could be produced in an experiment, and dipoles in the limit of an infinitely strong electric field. These simulations provide insight into what control we have over how the molecules collide at ultracold temperatures.

Dedication

For Team PhD, the greatest professional ARAM team in history.

Acknowledgements

I want to thank John Bohn for all of his help and support during this project, and for all of his terrible, terrible jokes. John has been a guiding light for me in all aspects of physics for the past fifteen months, and he has taught me so many important lessons about how one should investigate fundamental questions in science. I am a better physicist because of him.

I would also like to thank everyone in the Bohn Group, Reuben Wang, Eli Halperin, Dibyendu Sardar, and Hui Li, for giving me their attention, understanding my work, and helping me fix mistakes and improve my code. I want to specifically thank Eli Halperin for helping me understand how to numerically solve the Schrödinger equation. Everyone in the group has contributed in some way to improving this thesis, and I am extremely grateful for their patience and guidance.

Thank you to Jun Ye for agreeing to join my committee, and I hope this project is interesting and perhaps useful to you in some capacity. Thank you to Peter Mayr for being an excellent teacher, for indirectly leading me to pursue a Math minor, and for joining my committee as well.

Finally, thanks Mom and Dad for fostering my curiosity and perseverance from day one, and for giving me the autonomy to choose my own path. You are the reason I am here today, and the reason I am doing this. Thank you.

Contents

Chapter

1	Introduction: The Power of Ultracold Physics	1
1.1	Quantum Metrology	1
1.2	Quantum Simulators	2
1.3	Ultracold Chemistry	2
2	Background: Why Dipoles are Interesting	4
2.1	The General Set Up	5
2.2	Developing the Hamiltonian	8
3	Details of the Simulation	10
3.1	Julia vs. Matlab	10
3.1.1	Solving Efficiency	11
3.2	Carrying out the Calculations	11
3.2.1	Case 1: Freely Rotating Dipoles	14
3.2.2	Case 2: Applying an External Electric Field	18
3.2.3	Case 3: The Rigid Dipole Limit	23
4	Results and Conclusions	24
4.0.1	Description of AEPs	24
4.1	Trajectories in Physical Space	25

4.2	AEPs at various η	29
4.2.1	Details of Case 3	31
4.3	Plots of $\theta \cos \phi$ vs. η	33
4.4	Fraction of Convergent Paths	35
4.5	Conclusions and Looking Ahead	37
Bibliography		40

Figures

Figure

2.1	Dipole-Dipole Potential Contour Plot	5
2.2	Diagram of the Set Up	6
3.1	Choosing R_0 at $T_0 = 1 \mu\text{K}$	14
3.2	Choosing R_0 at $T_0 = 1 \text{mK}$	15
3.3	θ Probability Density for $E = 0$	20
3.4	θ Probability Density for $E = 5000 \text{V/cm}$	21
3.5	Collection of initial dipoles, $E = 0$	21
3.6	Collection of initial dipoles, $E = 5000 \text{V/cm}$	22
4.1	United Nations Logo	25
4.2	Physical Trajectories of Dipoles with $E = 0$	26
4.3	Physical Trajectories of Dipoles with $E = 5 \text{kV/cm}$	27
4.4	Physical Trajectories of Dipoles with $E \rightarrow \infty$	28
4.5	Landing Points for Cases 1, 2, and 3 at $\eta = 0, 30, \text{ and } 60^\circ$	30
4.6	Landing Points for Case 3 for η between 15° and 90°	32
4.7	Average final “x” values when $E = 0$	33
4.8	Average final “x” values when $E = 5 \text{kV/cm}$	34
4.9	Average final “x” values when $E \rightarrow \infty$	35
4.10	Number of Convergent Paths in Each Case	37

Chapter 1

Introduction: The Power of Ultracold Physics

For over 40 years now, experiments have been able to cool atoms to temperatures very close to absolute zero [1]. Since then, the field of ultracold physics has been consistently growing and improving, and in the last decade experiments have trapped and cooled molecules as well [2]. Current experiments can trap molecules and bring their temperatures down to the order of $1\ \mu\text{K}$ using a combination of laser cooling, evaporative cooling, and magneto-optical traps. Studying atoms and molecules in this ultracold regime opens a doorway to explore fundamental processes and unique quantum systems on the scale of relatively few interacting particles. The most common goals of investigating ultracold phenomena are improving quantum metrology, building quantum simulators, and understanding chemical reactions.

1.1 Quantum Metrology

The goal of quantum metrology is to use aspects of quantum theory such as entanglement and squeezed states to make extremely precise, sensitive measurements that could not be achieved in a classical framework. The quantum effects that enable such precise measurements are prominent in ultracold systems, so most applications of quantum metrology require atoms at ultracold temperatures. One popular application of quantum metrology is the development of optical atomic clocks, which keep time by measuring atomic transitions in the visible spectrum. Atoms are trapped in an optical lattice, and a fine tuned laser excites the atoms causing them to emit light [3]. Optical clocks are the most accurate method we know of measuring time, and their accuracy and stability have

been steadily increasing in recent years as improvements are made and new techniques discovered.

1.2 Quantum Simulators

Quantum simulators are another idea which can be explored in great detail in the ultracold regime. The goal of a quantum simulator is to use quantum bits to model complicated problems involving many interacting particles. These problems are poorly understood due to the incredible complexity of the quantum mechanics governing many body physics, and this complexity also makes conventional computers inadequate tools for simulating many body systems. Quantum simulators often function by trapping ions at ultracold temperatures and measuring the spin of the outermost electron of each ion as a qubit [4]. By hitting the ions with laser pulses at precise timings, the simulator can mimic interactions with quantum materials which are difficult to study explicitly. The interactions between qubits in the simulator are mathematically equivalent to a simplified model of real particles in unique materials, and the simulator allows the geometry of the simulated material to be manipulated freely by changing things like the lattice spacing.

1.3 Ultracold Chemistry

One other phenomenon which is often studied in the ultracold arena is chemical reactions. Typically chemical reactions are studied at temperatures and particle numbers where thermal variance causes a range of hundreds of kelvin in the reactants' initial temperatures, leading to many possible initial states. Reaction rates are then measured as the average over all of these initial states. However, with modern cooling and trapping techniques, molecules can be produced and controlled at ultracold temperatures, eliminating the thermal averaging present in previous experiments. Experiments can precisely control the initial conditions of ultracold trapped molecules, and this allows for comprehensive study of which initial conditions lead to reactions, and what pathways to reaction are taken from different starting points [5]. Understanding exactly what happens in chemical reactions and how the reactants initial conditions play a role could give us the ability to control chemistry manually in a way hitherto undreamt of by traditional chemists. This corner of

ultracold physics has been the focus of my research into dipolar collisions.

My project examining the long range interaction between two KRb molecules was undertaken with the long term goal of understanding to what degree we can control chemical reactions, and the immediate goal of probing the behavior of dipolar molecules immediately before they have a chance to react. I want to find out when the dipoles collide and when they are repelled away from each other; I also want to track how they are oriented when short range effects begin to take over, and if there is ever deviation from the familiar head-to-tail alignment. I chose to work with a classical model because, despite the accuracy of partial wave scattering theory, most researchers still imagine dipoles as little vectors in space pointing one way or another, and the calculations I do connect clearly to that mental image. This model does not claim to tell the full story, but it offers a clear and detailed starting point for many experiments or predictions. It is also useful as an indicator of where experimental limitations may lie regarding short range control.

Chapter 2

Background: Why Dipoles are Interesting

The focus of my project is the KRb molecule, which has a permanent electric dipole moment. The Potassium ion is slightly more electronegative than the Rubidium ion, so when the two atoms are bonded together, there is more positive charge near the Rubidium and a small internal electric field is generated. This results in a long range dipole-dipole interaction between reactants which is not present in single atom reactants or non-polar molecules like homonuclear diatoms (ex. N₂ or O₂).

The potential energy of the two dipoles is

$$V_{dip} = \frac{\vec{d}_1 \cdot \vec{d}_2 - 3(\vec{d}_1 \cdot \hat{r})(\vec{d}_2 \cdot \hat{r})}{r^3} \quad (2.1)$$

where \vec{r} is the vector distance between the dipoles, and \vec{d}_1, \vec{d}_2 are the dipole moments of molecules 1 and 2 [6]. If we write

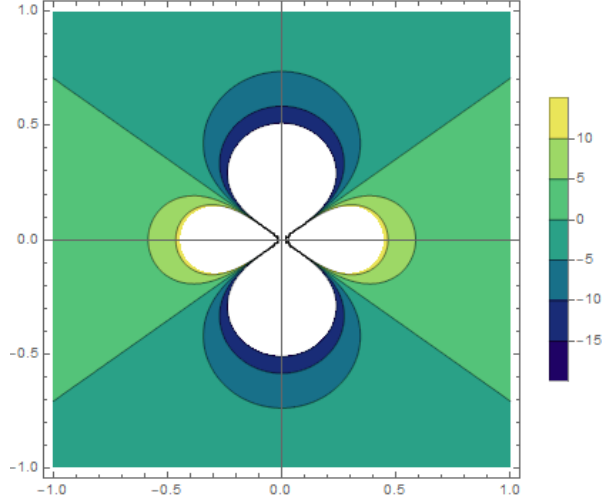
$$\vec{r} = r \sin(\eta) \cos(\beta) \hat{x} + r \sin(\eta) \sin(\beta) \hat{y} + r \cos(\eta) \hat{z} \quad (2.2)$$

for the relative distance vector, we can express V_{dip} as a function of the polar angle η and radius r at a fixed azimuthal angle $\beta = 0$ when both moments point in the z direction:

$$V_{dip} = \frac{d^2}{r^3} [1 - 3 \cos^2(\eta)] \quad (2.3)$$

We see that the long range dipole-dipole force results in anisotropic interactions between the reactants. When two dipoles are aligned head-to-tail, the force is attractive and the energy barrier is

Figure 2.1: Contour Plot of Equation 2.3, showing the strength of the potential between two dipoles both pointing in the $+z$ direction in arbitrary units. The straight diagonal lines represent $V = 0$, where the force switches from being attractive to repulsive. The lines are at an angle η of $\cot^{-1}(\frac{1}{\sqrt{2}}) = 54.74^\circ$ from the z axis.



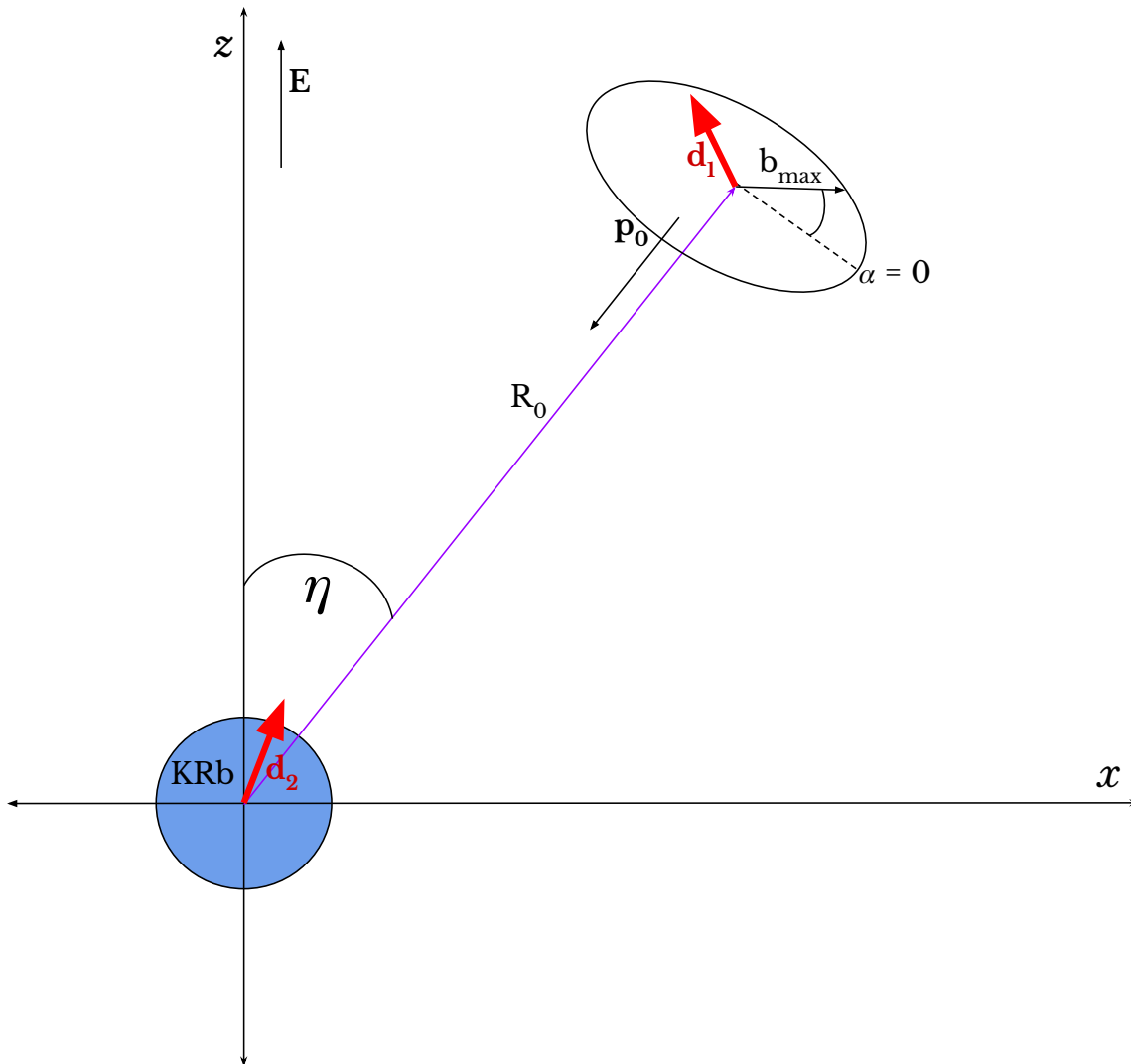
lowered, increasing the reaction rate. On the other hand, if the dipoles are stuck side-by-side with the same polarization, the force is repulsive and the reaction rate is diminished.

The orientation of dipoles can be controlled by changing the shape of the trap or adding an external electric field, and in this way reactions between dipolar molecules can be controlled with a high degree of precision. This thesis investigates how an external electric field affects the long range behavior of two KRb molecules. Three cases are studied: 1) zero applied field and freely rotating dipoles, 2) an intermediate applied field of 5 kV/cm which restricts the range of rotations, and 3) dipoles perfectly polarized along a given axis with no freedom to rotate. Case 3 can be thought of as the limit of the external field strength becoming infinitely strong.

2.1 The General Set Up

In all three cases, the interaction being studied is the same. The two molecules start separated by a large distance R_0 and drift toward one another very slowly. In the first two cases, the

Figure 2.2: A diagram labelling the initial variables in a general interaction with a finite electric field in the z direction (not to scale). The initial picture is nearly 2-dimensional, but the uncertainty disk around dipole 1 is parallel to the y axis and actually extends out of and into the page slightly.



molecules start at a temperature of 1 mK, or about 86 nano-electron volts of collision energy. This temperature is chosen because it is near the energy scale of some experiments, and the accuracy of the numerical solutions is not consistent at lower temperatures for the cases which allow for rotation. In the simpler third case, the temperature can be brought down all the way to 1 μ K, or about 86 pico-electron volts of energy. 1 μ K is a very common temperature range in ultracold

experiments [7]. It is often convenient to talk about energy in units of K because temperature can be more intuitive, and kinetic energy is directly proportional to temperature through Boltzmann's constant.

2.2 encapsulates every interaction being studied; as drawn, it represents the most general case 2, but as \vec{E} is reduced to zero or raised to infinity, the other special cases arise. In all three cases, we watch the molecules approach each other until either a) the distance between them is less than the molecular van Der Waals radius, where short range quantum effects start taking over, or b) enough time passes that the molecules are clearly never going to reach this short range region. For the sake of clearer visualization and simpler equations, the collision is studied in the Center of Mass (CM) frame with one of the dipoles sitting at the origin and the other molecule moving relative to the first. The two particles are always physically contained in a single plane, and we call the plane containing both dipoles at time 0 the x-z plane. Because the molecules always start the same distance apart, and they are initially in the x-z plane, the relative position of dipole 1, which is not at the origin, is determined by an angle η drawn with respect to the x axis.

The dipole-dipole force only depends on the distance between the dipoles and the angles of the two dipole moments, which means we only need to vary η in the x-z plane between $-\pi$ and π to study all the positions of dipole 1. Furthermore, any scenario with $\eta < 0$ can be thought of instead as a scenario with dipole 1 at the origin and dipole 2 at $-\eta$. Because the two dipoles are identical, any frame of reference with $\eta < 0$ can be transformed to a frame with $\eta > 0$ without changing the physics, so we only need to consider η between 0 and π to see every possible physical scenario. In the case of zero external field, the physics is also independent of η , and only the relative distance and internal angles need to be specified. When we add an electric field $\vec{E} = E\hat{z}$, however, varying η will generally affect the relative angle between the dipole moments. So far, the picture is completely classical, but to be more realistic we should acknowledge the effects of uncertainty in this interaction. Because we specify the collision energy without any uncertainty, the initial position of one of the dipoles can't be exact. The second dipole could really be anywhere in a small circular disk around the point (R_0, η) . The radius of this disk can be found using the uncertainty

principle:

$$\begin{aligned}\Delta x \Delta p &= \hbar \\ \Delta x * \mu \sqrt{\frac{2k_B T}{\mu}} &= \hbar \\ \Delta x &= \frac{\hbar}{\sqrt{2\mu k_B T}}\end{aligned}$$

This gives the radius of the disk of uncertainty in terms of the reduced mass μ and collision energy $k_B T$. To incorporate this uncertainty we will let Δx be the maximum impact parameter of dipole 1 and for each collision choose a random impact parameter and angle α within the disk. If we repeat this over many collisions, we get a distribution of initial impact parameters representing the smallest set of initial conditions allowed by uncertainty. We can think of this collection of initial conditions as representing an initial wave packet with equal probability of being measured anywhere within the uncertainty disk. Now that we've established this set up, we will use it as a starting point for each of the three cases we want to study.

2.2 Developing the Hamiltonian

The classical Hamiltonian contains a potential term and a kinetic term. In the CM frame, the kinetic term includes relative translational energy as well as the rotational energies of both dipoles:

$$K = \frac{p^2}{2\mu} + \frac{L_{\theta_1}^2 + L_{\theta_2}^2}{2I} + \frac{L_{\phi_1}^2}{2I \sin^2(\theta_1)} + \frac{L_{\phi_2}^2}{2I \sin^2(\theta_2)} \quad (2.4)$$

In Equation 2.4, p is the magnitude of the relative linear momentum, μ is the reduced mass, I is the moment of inertia of a single KRb molecule, and each L_i is an angular momentum with respect to angle i . The potential part of the Hamiltonian includes the possible interaction with the external field, the van der Waals potential between the molecules, and the dipole-dipole energy:

$$V_{tot} = V_{dip} + V_{field} + V_{vdW} = \frac{\vec{d}_1 \cdot \vec{d}_2 - 3(\vec{d}_1 \cdot \hat{r})(\vec{d}_2 \cdot \hat{r})}{r^3} - (\vec{d}_1 \cdot \vec{E} + \vec{d}_2 \cdot \vec{E}) - \frac{C_6}{r^6} \quad (2.5)$$

In terms of general coordinates this becomes

$$\begin{aligned}
 V_{tot} &= \frac{d^2}{r^3} [\sin \theta_1 \sin \theta_2 \cos (\phi_1 - \phi_2) + \cos \theta_1 \cos \theta_2] \\
 &\quad - 3 \frac{d^2}{r^5} [\sin \theta_1 \cos \phi_1 x + \sin \theta_1 \sin \phi_1 y + \cos \theta_1 z] \\
 &\quad \times [\sin \theta_2 \cos \phi_2 x + \sin \theta_2 \sin \phi_2 y + \cos \theta_2 z] \\
 &\quad - dE(\cos \theta_1 + \cos \theta_2) - \frac{C_6}{r^6},
 \end{aligned} \tag{2.6}$$

where C_6 is a constant and x, y , and z are Cartesian components of the separation vector \vec{r} , so $r = \sqrt{x^2 + y^2 + z^2}$.

Chapter 3

Details of the Simulation

3.1 Julia vs. Matlab

Our initial plan for finding particle trajectories was to simply use Matlab's built in differential equation solver `ode45` to solve the equations of motion resulting from the Hamiltonian from chapter 2. However, we quickly realized that the solutions calculated in Matlab were not conserving energy and were thus unphysical. We switched to using a new computing environment, Julia, which is optimized for doing computational science. The Julia package `DifferentialEquations.jl` comes with dozens of different integrators ranging up to 12th order with both Runge-Kutta and symplectic methods. An explicit, symplectic (fixed time step), 8th order integrator called `McAte8` was chosen to compute trajectories. `McAte8` is generally able to conserve energy to at least 1 part in 10^3 in our calculations. `McAte8` is part of the `DifferentialEquations.jl` package, and `DifferentialEquations.jl` also contains `DiffEqPhysics.jl`, which can read a Hamiltonian and automatically create the appropriate equations of motion. This means we only need to specify the Hamiltonian, initial conditions, and time span over which to solve, and `McAte8` will give us the trajectories in Julia.

Julia is not, however, optimized for displaying plots or generally showing results visually. Matlab is great at making plots and has many useful built in visualization tools, so after solving for the trajectories in Julia, we write the solutions to `.csv` files and use Matlab to interpret and represent the collected data.

3.1.1 Solving Efficiency

Because the solver McAte8 is a symplectic integrator, it uses a fixed time step which is prescribed at the start. This is not ideal for our problem because the necessary precision for the majority of the collision is relatively small, and we'd like to use larger time steps to save computing time, but in the final few hundred au, the forces become much stronger and the time step needs to be very small to get an accurate solution. To handle this dilemma, we divide the solution into a few regions. The first region has a time span on the order of those estimated above, and a large time step of maybe 1/1000th or 1/10000th the time span. The equations of motion are solved with this time span and time step until the separation r is about $\frac{R_0}{4}$. Then the solver stops, and the final coordinates of that calculation are used as initial values for a new solution, with a shorter time span and smaller time step. The problem is further divided in this way and the time step reduced at $r \approx \frac{R_0}{20}$ and then usually again at $r \approx \frac{R_0}{100}$. By dividing up the problem like this, we can quickly compute how the particles move in the less interesting, large separation region and also get an accurate description of the motion at the closest range we study, where behavior is the least predictable.

This technique is best suited to case 3, when the dipoles aren't allowed to rotate, because the initial behavior in that regime is almost trivial. In cases 1 and 2, the dipoles rotate on time scales much smaller than the scales of their linear motion, so even the early motion needs to be tracked quite accurately. We can still divide up the solution to reduce the time step slightly in cases 1 and 2, but the solutions in general require smaller time steps and take much longer. This is also one of the reasons cases 1 and 2 are simulated at a higher temperature than case 3.

3.2 Carrying out the Calculations

The Hamiltonian is solved numerically for each of the three cases. Each case has its own script; they all do the same thing, find the relative coordinates and internal angles of each dipole as a function of time, but there are a few key differences which distinguish them. In each code, the first

things specified are all of the constant parameters relevant to the system. First a few fundamental values are defined explicitly: the mass of one KRb molecule, $M = 127$ amu; the magnitude of KRb's body-frame electric dipole moment, $d = 0.6$ Debye; and the bond length, $R_{eq} = 7.66$ bohr radii are defined. The initial energy in the CM frame $T_0 = k_B * 1 \text{ K} = 3.17 * 10^{-6}$ or $T_0 = k_B * 10^{-6} \text{ K} = 3.17 * 10^{-12}$ Hartree is also defined. Then, constants which are functions of these fundamental values are defined: The reduced mass in the CM frame is simply $\mu = \frac{M}{2}$, the initial relative velocity in the CM frame is

$$v_0 = \sqrt{\frac{2T_0}{\mu}}, \quad (3.1)$$

the moment of inertia of one KRb molecule is MR_{eq}^2 , the maximum impact parameter is

$$b_{max} = \frac{\hbar}{\mu v_0}, \quad (3.2)$$

and the van Der Waals radius of two KRb molecules is

$$R_{vdW} = \frac{1}{2} \left[\frac{2\mu C_6}{\hbar^2} \right]^{1/4}, \quad (3.3)$$

where for KRb, $C_6 = 16130$ is determined by quantum mechanics [8].

Finally, the initial radius R_0 must be chosen. R_0 needs to be a distance where the initial collision energy is much larger than the potential energy due to the dipole-dipole interaction. In this limit, the initial dipole-dipole potential can be neglected and the two particles can be treated as being infinitely far away. This radius is not hard to estimate, once we pick how small we want V_{dip} to be. If we want the initial collision energy to be 100 times larger than V_{dip} , we can express that condition and solve for r :

$$\begin{aligned} |V_{dip}| &= 0.01T_0 \\ \frac{2d^2}{R_0^3} &= 0.01T_0 \\ R_0 &= \left(\frac{2d^2}{0.01T_0} \right)^{1/3} \end{aligned} \quad (3.4)$$

For a temperature of 1 μK , as in case 3, this equation says R_0 should be about 15,000 atomic units (au). If instead the temperature is 1 mK, as in cases 1 and 2, we get $R_0 = 1500$ au, reduced by a factor of 10 in correspondence with the temperature going up by a factor of 1000.

We can also determine how large R_0 should be by taking a few known trajectories and seeing how they vary as R_0 changes. Once we reach the infinite separation limit, changing R_0 should have no effect on the resulting trajectory. To measure how the trajectories change, we first draw a little blue sphere around dipole 2 at the origin whose radius is the van Der Waals radius. This little blue sphere is where all of the trajectories which result in collisions will stop, and when they stop dipole 1 will have some final position on the surface of the sphere. We can characterize a given trajectory by its final position on the surface of this sphere with two angles θ and ϕ .¹ If we focus on one trajectory, and only vary R_0 , we only need to track how θ on the little blue sphere changes to see how the trajectory shifts.

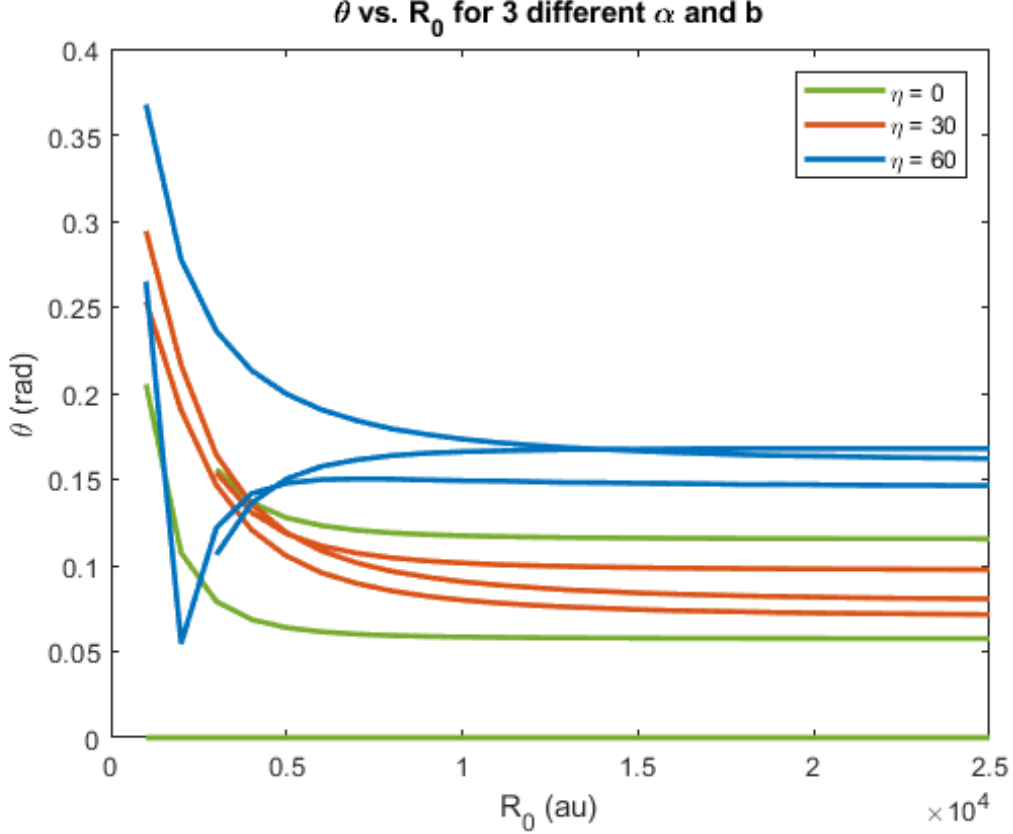
3.1 shows a plot of final angle θ vs R_0 at initial temperature of 1 μ K. There are nine curves plotted, each color represents a different initial η , and the three lines represent 3 different trajectories determined by their coordinates in the uncertainty disk, α and b . From this graph and the calculation, we chose to use $R_0 = 20,000$ au to safely ignore interactions between the dipoles initially.

The same style of plot is shown for an initial temperature of 1 mK in 3.2. It is very similar, and both plots show decent agreement with the calculation. It is important to note the calculation has a threshold of $V_{dip} = 0.01T_0$, and this is a threshold we chose. For the accuracy of our model, the potential being less than 1% of the collision energy is sufficient, as shown by the θ vs. R_0 plots, but other applications could require an even smaller potential energy initially.

With R_0 established for both the 1 mK and 1 μ K regimes, we can proceed to study the Hamiltonian and other solving parameters for each of the three cases.

¹ Note that these angles are different from the internal angles $\theta_1, \theta_2, \phi_1$, and ϕ_2 . θ is also in general different from η . There are a lot of angles to keep track of in this interaction.

Figure 3.1: The same few trajectories were calculated for R_0 varying from 1000 to 25000 au. We see at low values of R_0 , where V_{dip} and T_0 are comparable, the final angle changes wildly with R_0 . However, by the time R_0 is above 20,000 au, the change in θ is negligible.

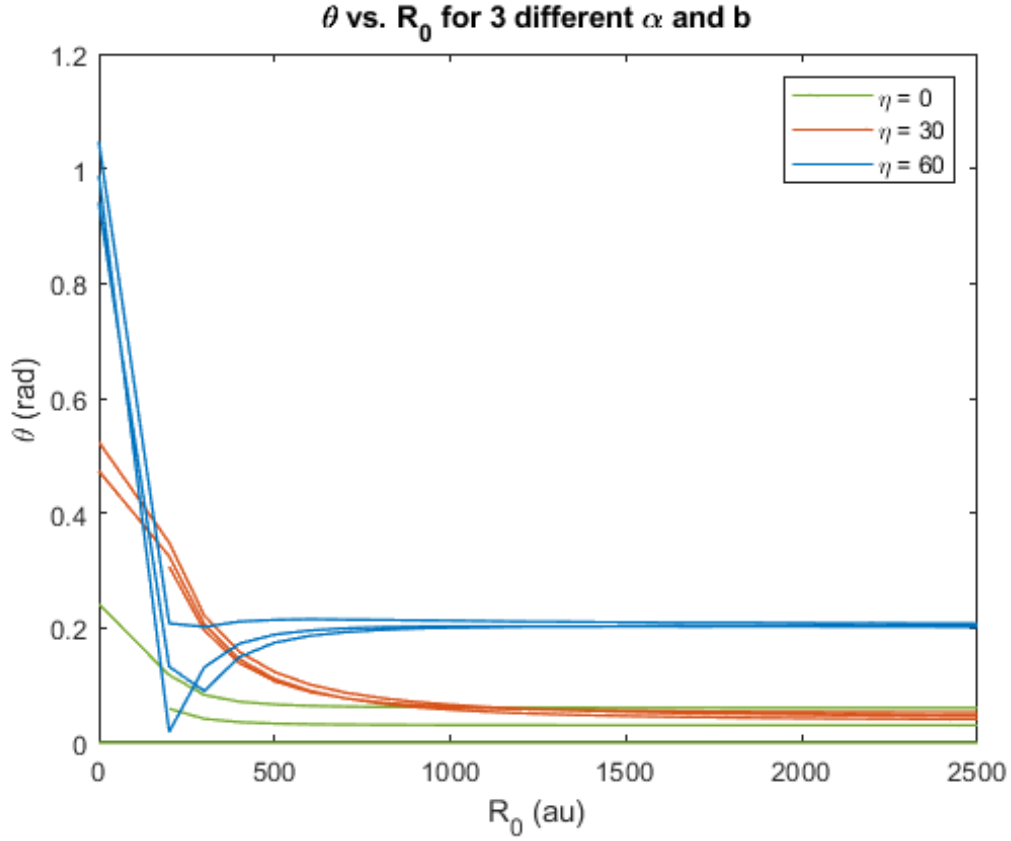


3.2.1 Case 1: Freely Rotating Dipoles

The first case is the simplest in principle, for it is the two dipoles moving according to each other's influences without outside intervention. This is meant to represent two KRb molecules in the ground state approaching each other from infinitely far away. The only relevant variables are the internal angles of each dipole and the distance between them. The dipoles are expected to naturally align head-to-tail quite easily, because their initial energy is low and they come together very slowly.

The Hamiltonian is written in explicitly as a function $\mathcal{H}(\vec{p}, \vec{q})$, where \vec{p} and \vec{q} are vectors containing seven coordinates, three for relative position/momentum and two for the internal angles

Figure 3.2: Similar to the previous figure, but the scale of the R_0 axis is reduced by a factor of 10. Again at low values of R_0 the final angle changes wildly with R_0 , and once R_0 is above 2,000 au, the change in θ is negligible.



of each dipole:

$$\vec{p} = \begin{bmatrix} p_x \\ p_y \\ p_z \\ L_{\theta_1} \\ L_{\phi_1} \\ L_{\theta_2} \\ L_{\phi_2} \end{bmatrix} \quad \& \quad \vec{q} = \begin{bmatrix} x \\ y \\ z \\ \theta_1 \\ \phi_1 \\ \theta_2 \\ \phi_2 \end{bmatrix} \quad (3.5)$$

In the script for case 1, the Hamiltonian has no $V_{field} = -dE(\cos \theta_1 + \cos \theta_2)$ term because the

strength of the electric field is zero. The Hamiltonian in case 1 is then

$$\mathcal{H}_1 = K + V_{dip} + V_{vdW} \quad (3.6)$$

with K from Equation 2.4 and $V_{dip} + V_{vdW}$ from Equation 2.5. The goal is to use this Hamiltonian to find trajectories over a large ensemble of initial conditions. In the code, two for loops are used to cycle through many different initial conditions. The first loop varies the angle η in the x-z plane from 0 to 90° . Within this loop over different η values, the second loop varies the initial position within the uncertainty disk. At each iteration in the second nested loop, a random impact parameter between zero and b_{max} is chosen along with an angle α between 0 and 2π . Initial internal angles θ_1, ϕ_1, ϕ_2 are also chosen randomly within their range. Similar to the argument allowing us to limit η between 0 and $\frac{\pi}{2}$, the second polar angle θ_2 doesn't actually need to vary at all,² and we choose to initially set $\theta_2 = \frac{\pi}{4}$ for all case 1 calculations.

Besides the initial internal angles, we also need to choose the initial position of dipole 1 relative to dipole 2 in a way consistent with our established initial radius R_0 , relative angle η , and uncertainty disk. With the random impact parameter b and angle α , we can write the “x” and “y” coordinates of dipole 1 within the uncertainty disk accordingly:

$$x_d = b \cos \alpha \quad (3.7)$$

$$y_d = b \sin \alpha \quad (3.8)$$

With these coordinates and R_0 , we set the initial Cartesian position of dipole 1 to be

$$x_i = x_d \cos \eta + R_0 \sin \eta \quad (3.9)$$

$$y_i = y_d \quad (3.10)$$

$$z_i = R_0 \cos \eta - x_d \sin \eta. \quad (3.11)$$

These coordinates demonstrate the fact that besides the y displacement due to uncertainty, our initial picture is entirely 2 dimensional, and they also show how the disk itself moves from being centered on the z axis at $\eta = 0$ to the x axis at $\eta = \frac{\pi}{2}$.

² Of course either one of the two angles can be held fixed, there's nothing special about θ_2 , but since dipole 2 is held at the origin in our frame of reference, it makes sense to vary θ_1 and fix θ_2 .

Because we are modelling the ground state, with $n = 0$ and hence $l = 0$, the angular momenta of both dipoles should be zero. However, because we are using a classical model to describe a quantum state, we have to account for the uncertainty in the angular momentum the same way we did for the position. In quantum mechanics, a particle has $l = 0$ and $L = 0\hbar$ in the ground state, and when excited to $l = 1$, the particle gains $L = 2\hbar$ angular momentum. This means that classically, a particle in the ground state can actually have any angular momentum less than $L = 1\hbar$ before being excited to the $l = 1$ state. To account for this, initial total angular momentum of each dipole is chosen in a random direction at angle τ with respect to the z axis and given random magnitude L_0 between zero and one ($\hbar = 1$ in atomic units). The θ and ϕ components of \vec{L} are then determined by vector addition and trigonometry. If $\hat{\rho}$ is the direction of \vec{L} perpendicular to the z axis, then

$$\vec{L} = L_0 \sin(\tau)\hat{\rho} + L_0 \cos(\tau)\hat{z}, \text{ and}$$

$$L_{\theta,i} = \vec{L} \cdot \hat{\rho} = L_0 \sin(\tau) \tag{3.12}$$

$$L_{\phi,i} = \vec{L} \cdot \hat{z} = L_0 \cos(\tau). \tag{3.13}$$

The initial linear momentum depends on the reduced mass and the collision energy and varies with η because the dipoles are always initially aimed directly at each other in the CM frame.

$$p_{x,i} = -\mu v_0 \sin \eta \tag{3.14}$$

$$p_{y,i} = 0 \tag{3.15}$$

$$p_{z,i} = -\mu v_0 \cos \eta \tag{3.16}$$

Regarding the physical model, we are technically ready to solve, having the Hamiltonian and knowing the necessary initial conditions. For the integrator to proceed, however, we still need to specify the time step and total time span to solve over. In looking for the total time span, we can get a rough overestimate by assuming there were no forces, and the dipoles were just drifting

toward each other at their initial speeds until they collide. The collision would then take

$$\begin{aligned} t_{1\mu K} &\lesssim \frac{R_{0,1\mu K}}{v_{0,1\mu K}} \\ &= 2.7 * 10^{12} \text{ atomic time units or } 65 \mu s \end{aligned}$$

for dipoles at $T_0 = 1\mu K$, and

$$\begin{aligned} t_{1mK} &\lesssim \frac{R_{0,1mK}}{v_{0,1mK}} \\ &= 8.6 * 10^9 \text{ atomic time units or } 21 \mu s \end{aligned}$$

for dipoles at $T_0 = 1mK$. These estimates are used as the initial time spans for each regime. The time step is determined mainly by trial and error. We start around 1/1000th of the time span, and then test this step size in a few calculations to see if energy is conserved. The time step is gradually reduced as necessary until energy is conserved to about 1 part in 10^6 for the vast majority of calculations. Once all of these conditions are set, we solve an ensemble of hundreds or thousands of initial conditions and analyze statistics and patterns in the data in Matlab.

3.2.2 Case 2: Applying an External Electric Field

In the second case, we turn on an electric field with strength of our choosing, up to the maximum of what can be reasonably produced in an experiment. The initial azimuthal angles ϕ_1 and ϕ_2 are still chosen randomly, but the polar angles are chosen according to the initial θ wavefunction which depends on the strength of \vec{E} . The Hamiltonian for a single dipole in an external field is

$$\mathcal{H}(\theta) = \frac{L_\theta^2}{2I} - \vec{d} \cdot \vec{E} \quad (3.17)$$

with θ being the angle between the dipole moment and the electric field. In quantum mechanics, L_θ^2 is replaced with the operator $-\hbar^2 \frac{1}{\sin\theta} \frac{\partial}{\partial\theta} (\sin\theta \frac{\partial}{\partial\theta})$, the polar angular part of the Laplacian. Writing this and doing the dot product in the potential term, the Hamiltonian operator becomes

$$\hat{\mathcal{H}}\psi = \frac{-\hbar^2}{2I} \frac{1}{\sin\theta} \frac{\partial}{\partial\theta} (\sin\theta \frac{\partial\psi}{\partial\theta}) - dE \cos\theta\psi. \quad (3.18)$$

Eigenfunctions are found by diagonalizing a matrix approximation of this Hamiltonian. The angular momentum term can be expanded by applying the outer derivative:

$$\frac{-\hbar^2}{2I} \frac{1}{\sin \theta} \frac{\partial}{\partial \theta} \left(\sin \theta \frac{\partial \psi}{\partial \theta} \right) = \frac{-\hbar^2}{2I} \left(\cot \theta \frac{\partial \psi}{\partial \theta} + \frac{\partial^2 \psi}{\partial \theta^2} \right) \quad (3.19)$$

With the Hamiltonian expanded in this way, the three terms can each be expressed approximately as a matrix. For the derivatives of ψ , we treat the variable θ like a discrete value between 0 and π on a grid with N different grid points. This is an approximation that becomes more accurate as more grid points are added. The second derivative $\frac{\partial^2 \psi}{\partial \theta^2}$ evaluated at $\theta = \theta_n$ can then be written as

$$\frac{\partial^2 \psi}{\partial \theta^2} \approx \frac{\psi(\theta_{n+1}) + \psi(\theta_{n-1}) - 2\psi(\theta_n)}{(\Delta\theta)^2}, \quad (3.20)$$

and the first derivative

$$\frac{\partial \psi}{\partial \theta} \approx \frac{\psi(\theta_{n+1}) - \psi(\theta_{n-1})}{\Delta\theta} \quad (3.21)$$

where $\Delta\theta$ is the grid spacing. Approximating θ as a discrete variable allows us to write the Hamiltonian as an $N \times N$ matrix with the following elements:

$$\hat{\mathcal{H}}_{i,i-1} = \frac{1}{I(\Delta\theta)^2} + \frac{\cot \theta}{4I\Delta\theta} \quad (3.22)$$

$$\hat{\mathcal{H}}_{i,i} = \frac{-1}{2I(\Delta\theta)^2} - dE \cos \theta \quad (3.23)$$

$$\hat{\mathcal{H}}_{i,i+1} = \frac{1}{I(\Delta\theta)^2} - \frac{\cot \theta}{4I\Delta\theta} \quad (3.24)$$

with $\hbar = 1$. Diagonalizing this matrix gives us energy eigenstates of the Hamiltonian which depend on the field strength E . We expect both particles to initially be in the lowest energy eigenstate. For no electric field, the probability density in θ is uniform, and in spherical coordinates the total θ part of the probability integral, which is $|\Psi|^2 \sin \theta$, looks like a pure sine wave. When an external field is applied, the sine wave is distorted and shifted to favor θ along the axis of the external field. Probability densities for electric field strength $E = 0$ and $E = 5000$ V/cm are shown in 3.3 and 3.4, and the endpoints of an ensemble of initial dipoles chosen according to these distributions are shown in 3.5 and 3.6.

In the code, initial values of θ are chosen according to these distributions based on the strength of the external field. Besides the initial θ distribution, most of the solving in Case 2 is the same as in Case 1. The only other difference is that in Case 2, because the electric field points along the z axis, changing the angle η will in general affect how the dipoles are oriented relative to the applied field. The η values chosen vary by 15 degree increments from the minimum 0 to the maximum 90 degrees.

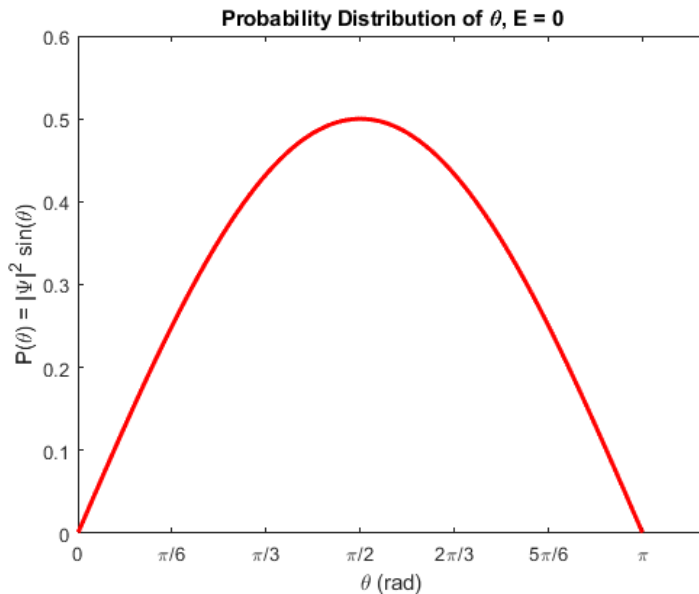


Figure 3.3: The spherical probability density of the polar angle θ when there is zero external electric field. The sine wave peaks at $\theta = \frac{\pi}{2}$ because on the sphere, the circumference of the cross sectional circle at $\theta = \frac{\pi}{2}$ is largest.

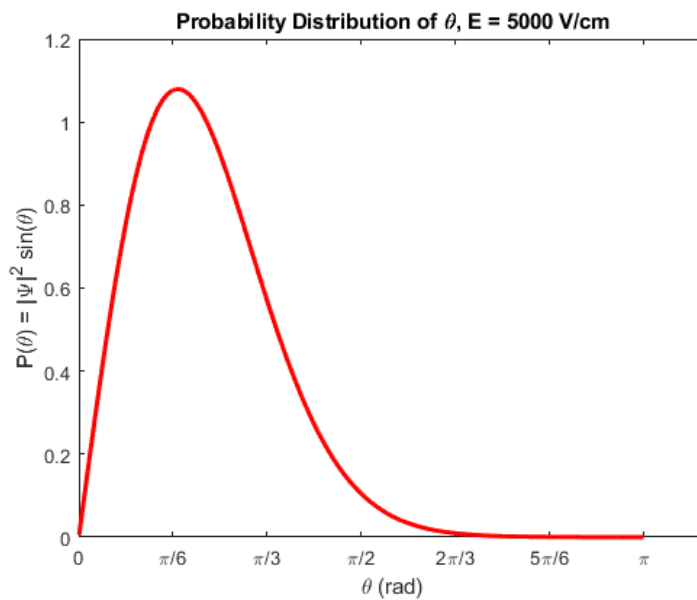


Figure 3.4: The spherical probability density of the polar angle θ when there is a 5 kV/cm applied field in the z direction. The distribution shifts toward $\theta = 0$ to minimize the potential energy. The probability density still approaches zero at $\theta = 0$ because on the sphere, the circumference of the cross sectional circle at $\theta = 0$ goes to zero.

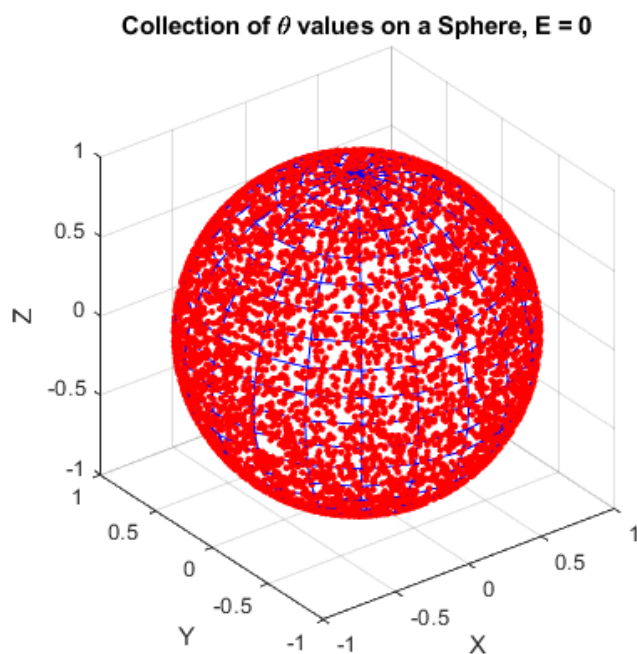


Figure 3.5: Each red dot represents the endpoint of an initial dipole moment with its polar angle θ chosen according to the probability density, and its azimuthal angle ϕ chosen randomly. The dipoles appear uniformly dispersed across the sphere.

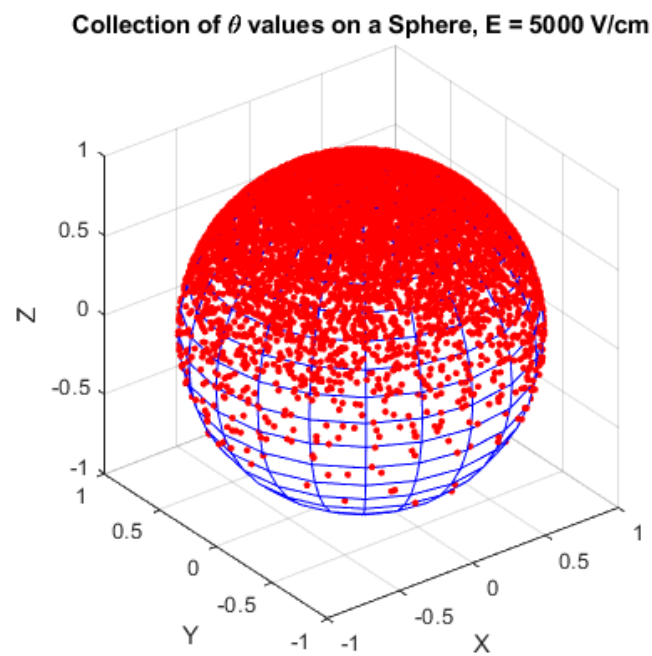


Figure 3.6: When the electric field is turned up to 5000 V/cm, the dipoles are more densely concentrated near the north pole, and very sparse below $\theta = \frac{\pi}{2}$.

3.2.3 Case 3: The Rigid Dipole Limit

In this final case, the electric field is taken to be so strong that the dipoles have no rotational degrees of freedom and are forced to always point in the z direction. This allows us to make many simplifications to the form of the dipole-dipole term in the Hamiltonian by setting all polar angles θ_i equal to zero.

$$\begin{aligned} V_{dip}(\theta_1 = \theta_2 = 0) &= \frac{d^2}{r^3} - 3\frac{d^2}{r^5}[z^2] \\ &= \frac{d^2}{r^5}(x^2 + y^2 - 2z^2) \end{aligned} \quad (3.25)$$

The kinetic term also reduces to simply $\frac{p^2}{2\mu}$, because the rigid dipoles don't pick up any rotational energy during their collision. The total Hamiltonian in case 3 is then

$$\mathcal{H} = \frac{p^2}{2\mu} + \frac{d^2}{r^5}(x^2 + y^2 - 2z^2) - \frac{C_6}{r^6} \quad (3.26)$$

Because this Hamiltonian is so simple, the calculations in case 3 can be done much faster and are accurate at much lower temperatures, which is why the data we collected for case 3 is at a temperature of 1 μK instead of the 1 mK data for cases 1 and 2.

With each case established and the code laid out, we can now analyze the results of these simulations.

Chapter 4

Results and Conclusions

After considering several different approaches to data representation, We decided to look at a combination of paths in physical space, azimuthal equidistant projections (AEPs) of the final positions, measurements of the average final polar angle, and the fraction of paths which converge and reach the little blue sphere. The plots in physical space show the actual path a given particle took in the CM frame during the interaction, and I think they are the most intuitive way to see what the trajectories are doing. The AEPs give crucial information about how the dipoles collide and how focused or sporadic the collection of converging trajectories is. These projections along with graphs of the final polar angle tell us how the dipole are most commonly oriented when their short range interactions begin to dominate. The fraction of convergent paths also helps us understand if the interaction is mostly attractive or repulsive, and how it depends on the angle η .

All of the plots shown for cases 1 and 2 are made from a data set containing 500 attempted collisions per η at three different η values: 0, 30, and 60°. Of the 1500 total trajectories in each case, roughly 90% conserved energy to at least 1 part in 10³. In the future, more data will be collected for these cases at more varied values of η . The plots for case 3 are made from a data set containing up to 2000 attempted collisions per η at 7 evenly spaced η values between 0 and 90°.

4.0.1 Description of AEPs

An AEP is a way to visualize points of a sphere on a flat disc: the north pole, or the point lying exactly on the z axis of the sphere, becomes the center of the disc, and concentric rings around

the center are like latitude lines on the earth, circles which are equidistant from the north pole. This means that the radius of the disc represents the polar angle θ measured with respect to the z axis. The most famous example of an AEP is probably the logo for the United Nations, shown in 4.1.



Figure 4.1: A familiar instance of azimuthal equidistant projection is in the logo for the United Nations. Alaska, Greenland and the Arctic region are near the center of the plot, and the rest of the globe spreads radially outward. Antarctica is not shown in the logo, but it would be smeared around the circumference of the plot since the south pole is technically mapped to every point on the circumference of the disc.

4.1 Trajectories in Physical Space

4.2 - 4.4 show collections of many trajectories in physical space in the CM frame for cases 1, 2, and 3. The little blue sphere is centered around dipole 2, and dipole 2 is kept at the origin for all calculations. This means that what is plotted shows the relative motion of the two dipoles leading up to their potential reaction.

In case 1, varying η doesn't affect the interaction, so the different collections of trajectories appear the same, simply shifting along the surface of the sphere. This is in contrast to cases 2 and 3, where different collections of initial conditions behave quite differently because of their unique orientation relative to the electric field. Case 1 has some trajectories which repel each other and don't reach the little blue sphere because the dipoles are rotating at different frequencies and when they approach each other, their fields are misaligned and they are pushed away.

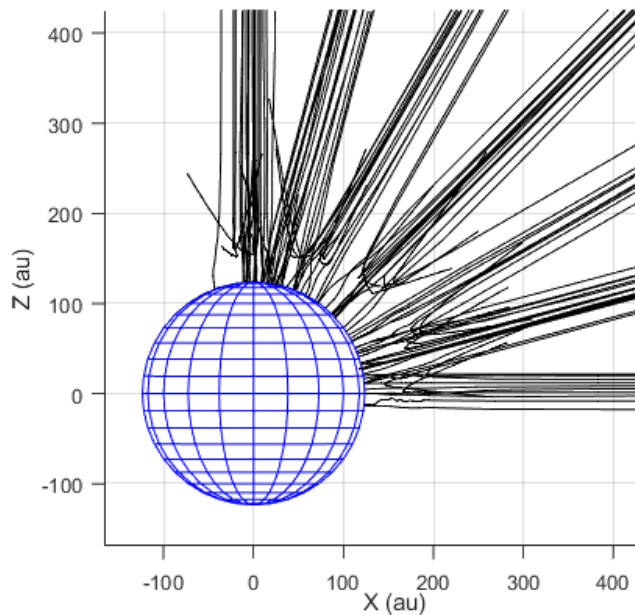


Figure 4.2: In case 1, the clusters exhibit similar behavior at various η because each cluster represents a set of random orientations, and there is no external field pushing the dipoles one way or another. The dipoles mostly just move straight toward each other and if their moments aren't too misaligned, they collide. There is some slight variance in each cluster because they are different randomly chosen points.

In case 2, the dipoles are classically oscillating around the z axis, and this means they are more likely to collide near the north pole of the little blue sphere. This effect is prominent at intermediate and small η , where we see the paths bend up toward the z axis near the blue sphere. We expected case 2 to look significantly more chaotic than case 1, but instead it appears quite orderly. The trajectories at very large η somehow also collide with the sphere without very much deflection. This may be because oscillating around the z axis causes the average dipole-dipole force to be very close to zero, and the dipoles essentially fly toward each other freely as if they were neutral particles.

Case 3 looks strikingly different from cases 1 and 2, which makes sense because the conditions of case 3 are much more restrictive. Because both dipoles are always pointed in the z direction, only those dipoles which are pushed toward the north pole quickly enough are able to collide successfully. We see many trajectories coming from large η which bend around dipole 2 but never

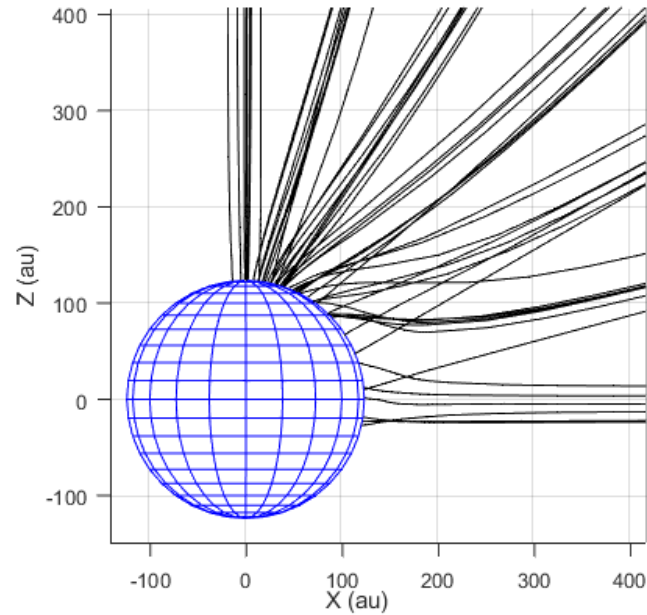


Figure 4.3: In case 2, we can see parts of the ensembles at intermediate η bending up toward the z axis. This is because the electric field is in the z direction, so both dipoles are more likely to be pointing in the z direction. At $\eta = 0$, the trajectories appear to be focused together near the north pole. At $\eta > 60^\circ$, some trajectories are drawn toward the north pole, but some are able to collide near the equator. We think this is because the dipoles spend equal amounts of time pointing toward and away from each other, and the attraction and repulsion between them average to zero.

enter the attractive regime of the dipole-dipole field, and end up missing the little blue sphere.

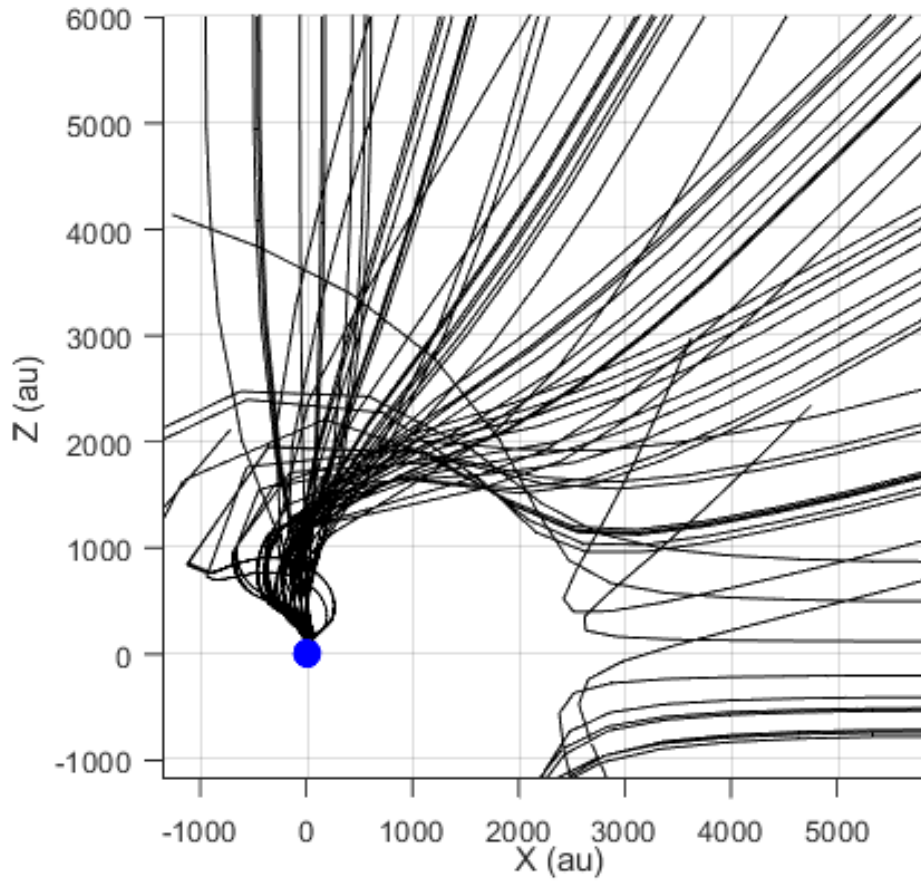


Figure 4.4: In case 3, we see all of the convergent paths focusing together near the north pole. This plot covers a much longer length scale because the data for case 3 was collected at lower temperatures. The lower temperature also means the initial ensembles in case 3 are spread over a larger uncertainty disc, so the clusters start overlapping earlier.

4.2 AEPs at various η

Our AEPs are shown in 4.5, representing landing points of the dipoles on the little blue sphere at the van der Waals radius. These landing points are the final calculated positions of the dipoles in the CM frame, and their radial position represents the final polar angle on the little blue sphere. The following figures show the landing points of a cluster of initial conditions in the three different cases side by side for $\eta = 0$, $\eta = 30^\circ$, and $\eta = 60^\circ$. The x axis in physical space and the x axis of the AEPs correspond, so as η is increased in the x-z plane, the point representing $\theta = \eta$ moves horizontally on the AEP.

We see that in case 1, the cluster is centered around the z axis at $\eta = 0$, and shifts toward $\theta = 30^\circ$ and $\theta = 60^\circ$ as η is shifted. This agrees with what we saw in the physical trajectories and what we expect for the case of zero external field. If the $\eta = 30^\circ$ and $\eta = 60^\circ$ plots were shown with the center of the AEP aligned with the axis in the η direction, they would look identical to the $\eta = 0$ plot.

This is in contrast to the case 2 plots, which stay tightly grouped together closer to the north pole, but also have a sort of tail of more wild landing points which aren't drawn toward the north pole very much. We believe this tail is a consequence of the fact that in a classical model, ideal dipoles are always oscillating around the direction of the field, and thus there are large intervals of time when both dipoles are pointed somewhat far away from the field axis, and they can still attract each other.

The radial axis is scaled differently in case 3 because the dipoles are always confined to a much tighter region near the north pole of the little blue sphere. All of the trajectories which manage to collide in case 3 do so within 35° of the z axis, whereas in cases 1 and 2, trajectories at large η can sometimes collide more than 90° away from the z axis, near the south pole. This is likely due to the fact that in the first two cases, dipole 2 is not stuck pointing in the z direction for all time.

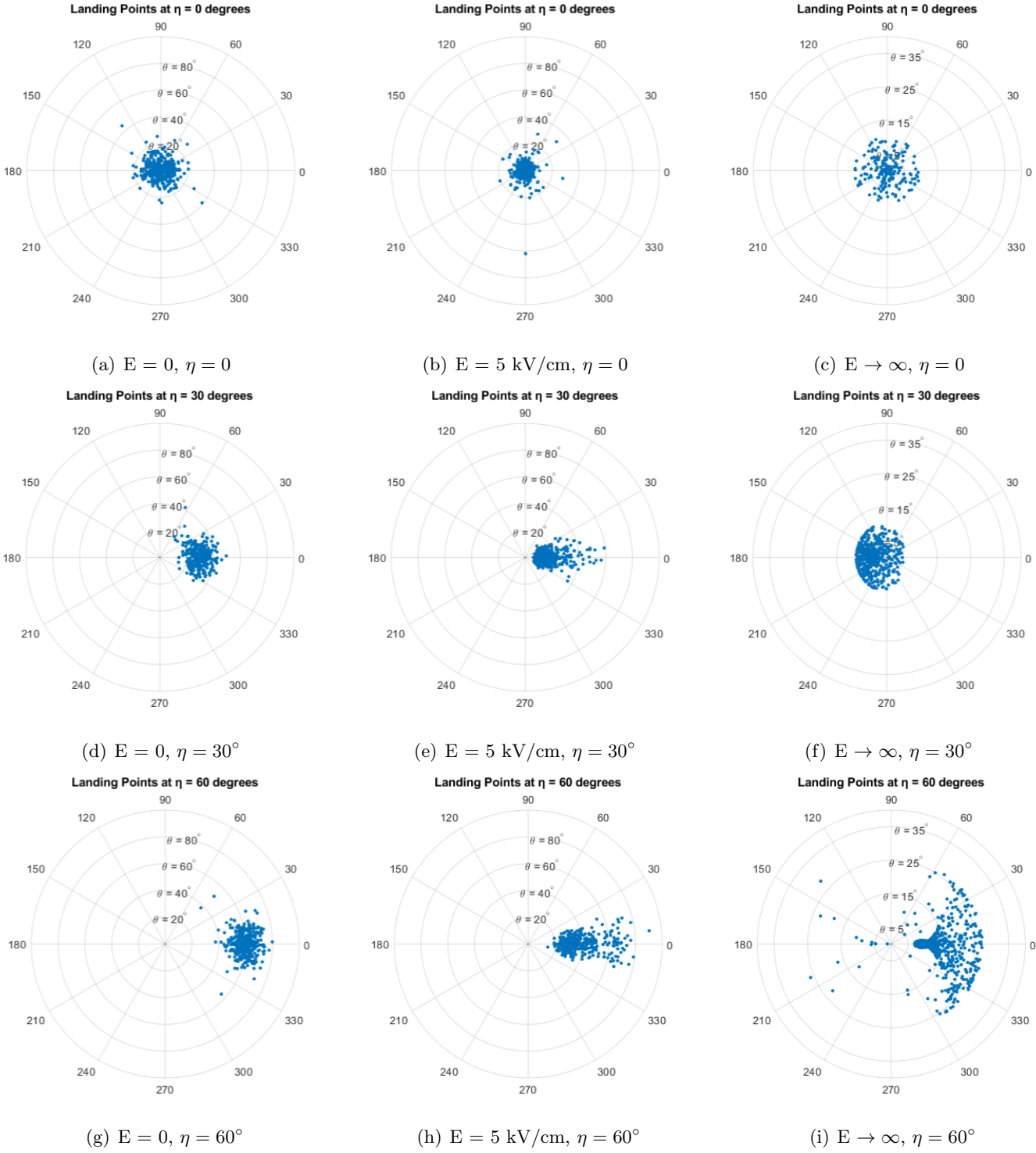


Figure 4.5: Landing points for all three cases at selected values of η . In case 1, the cluster largely maintains a uniform shape and only shifts its position. In case 2, the cluster picks up a sort of tail of dipoles nearer to the equator as η increases. In case 3, the cluster first shifts to the opposite side of the z axis, then shifts back and makes a much more complex shape. Notice that the polar θ axes are scaled differently in each case, so that even though the rigid case distribution looks more sporadic at $\eta = 60^\circ$, all of the points are still within 30° of the north pole.

4.2.1 Details of Case 3

Because case 3 is much simpler to model, more data was collected in this regime, and some strange patterns were found in the landing points of convergent trajectories when the dipoles are rigid. AEPs for more η values are shown at the end of this section. The main takeaway is simply that the dipoles are heavily focused in case 3, always landing within 35° of the north pole, but within this small 35° window, there is some very interesting structure.

At small η , the collection of landing points shifts toward the opposite side of the little blue sphere as η is increased. This indicates that trajectories are being deflected around the little blue sphere at first, but when they cross over into the attractive region of the dipole-dipole potential, they are pulled back and eventually land on the little blue sphere. At large enough η , however, this is no longer possible as the dipoles are moving too fast by the time the force becomes attractive, and the field is not strong enough to pull them back. At these large η values, the distribution shifts back to the familiar right side of the disc, and the clusters of random initial position vaguely resemble a nephroid, which is the shape traced by a point on a circle of radius a rolling around a larger fixed circle of radius $2a$. I do not yet have a reasonable explanation for these patterns.

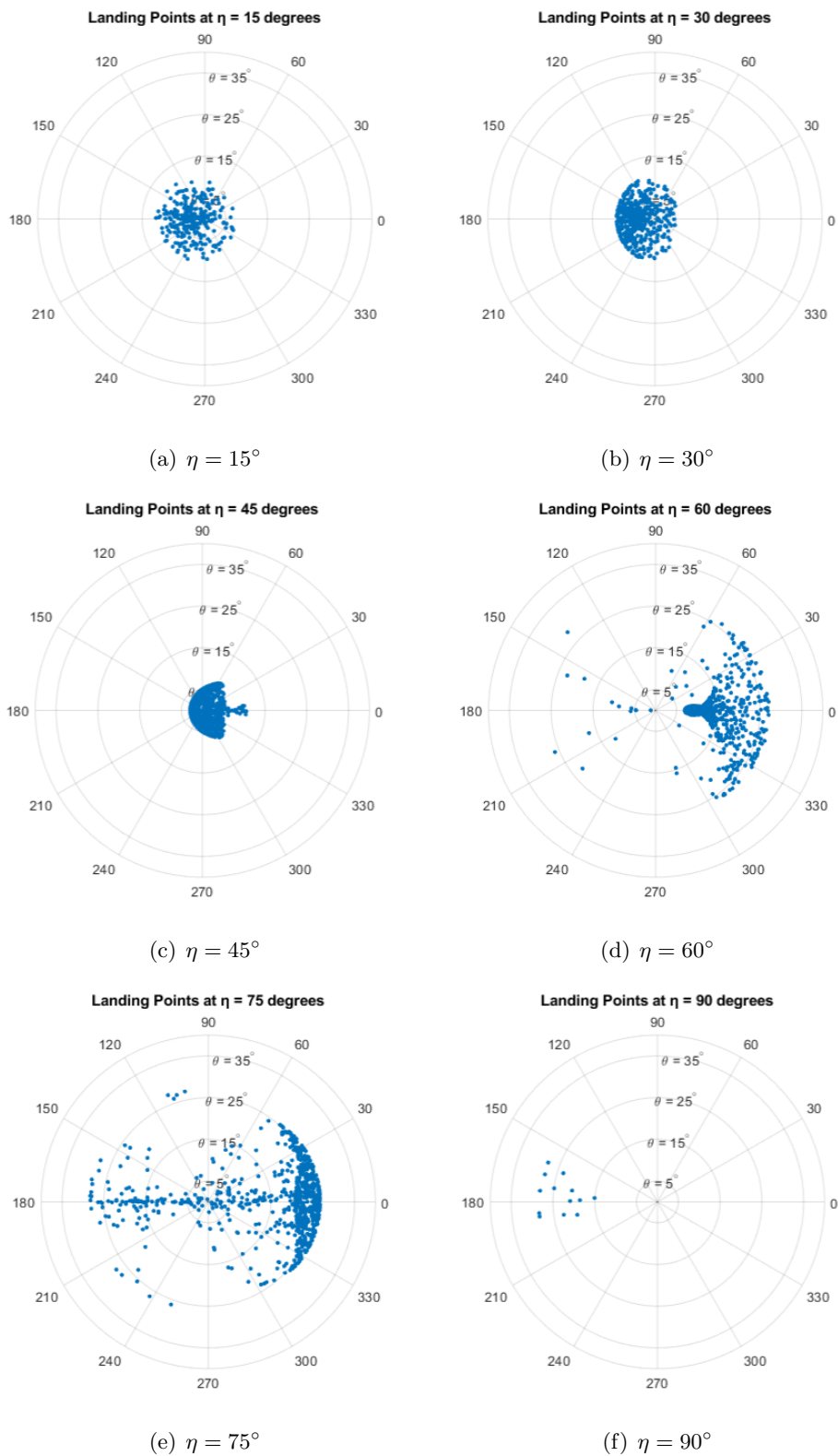


Figure 4.6: The landing points in case 3 make some very unpredictable patterns at large values of η .

4.3 Plots of $\theta \cos \phi$ vs. η

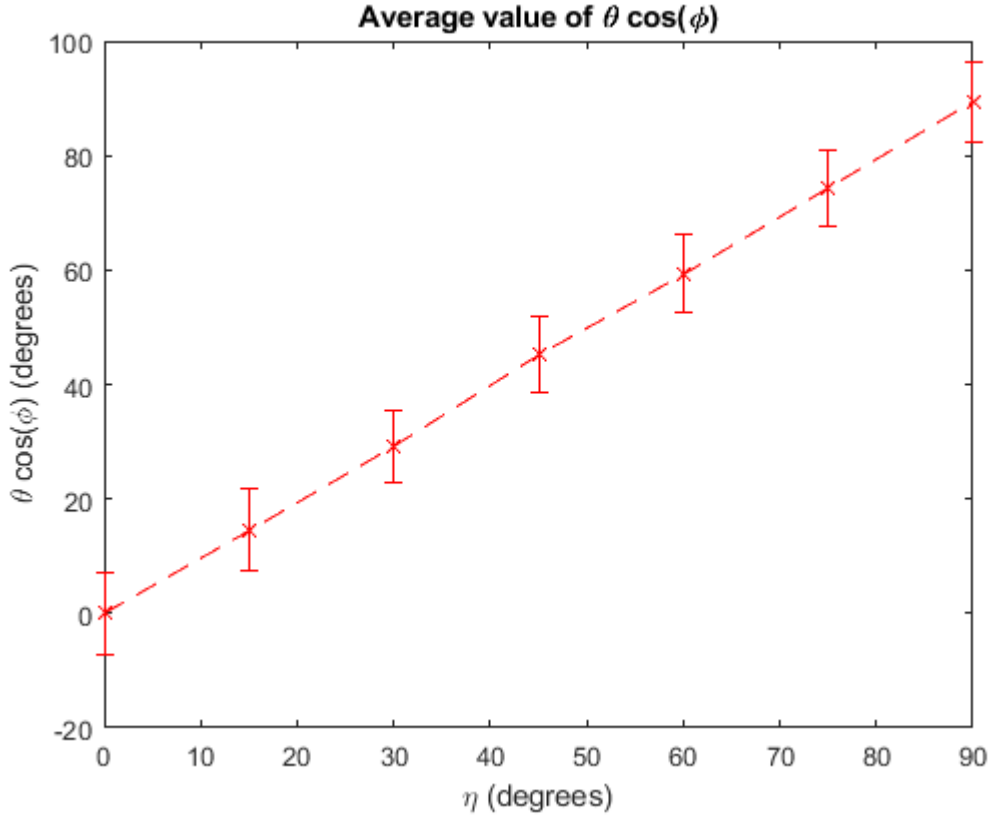


Figure 4.7: In case 1, the average value of $\theta \cos \phi$ is equal to η , and the plot is a straight line with slope 1. The error bars represent the spread of a given cluster, and these error bars are roughly constant, showing again that η doesn't affect the physics of the freely rotating dipoles.

These plots show the average value of $\theta \cos \phi$ for an ensemble of initial conditions at a specific angle η for all three cases. $\theta \cos \phi$ is essentially the x coordinate of a landing point on the azimuthal equidistant projection. The reason this quantity is plotted instead of simply graphing θ vs. η , is because of the natural spread of landing points around the north pole at small η . This spread is a result of the uncertainty in the initial position, and is important to show, but the spread means that in case 3, the average value of θ at $\eta = 0$ is greater than zero. This is counterintuitive because we expect everything to be centered around the north pole in this scenario, and indeed that is what we see in plot (c) of 4.5. By tracking $\theta \cos \phi$ instead, we have a quantity that does go to zero at $\eta = 0$ in case 3, and still maintains information about the final polar angle θ and the location of a

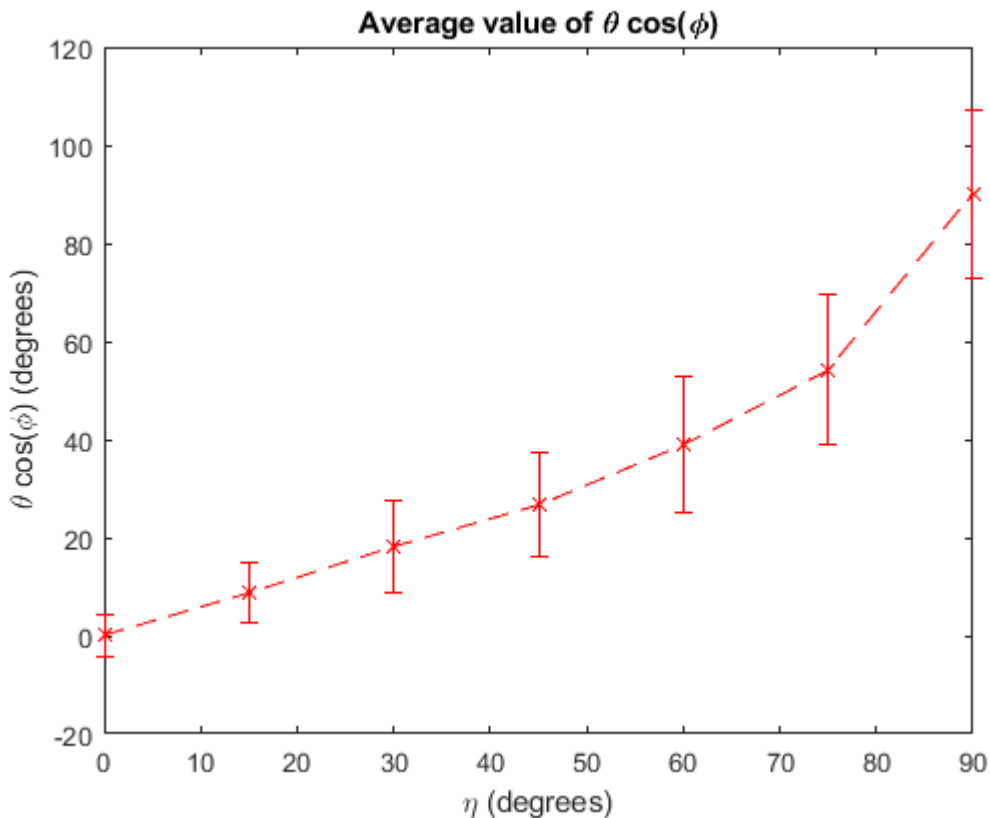


Figure 4.8: In case 2, the average value of $\theta \cos \phi$ is generally less than η because the dipoles are motivated to stay closer to $\theta = 0$, but $\theta \cos \phi$ still increases as η increases. The error bars also get wider at larger η , indicating the clusters of landing points are more spread out as the incoming dipole are moved away from the field axis.

given point on the little blue sphere.

By adding error bars which represent the standard deviation in the average value of $\theta \cos \phi$, we can also see from these plots how focused or spread out the dipoles are when they reach the van der Waals radius. The standard deviation is smallest in case 3, which has the heaviest focusing influence with an extremely strong external field. Case 2 has the largest standard deviation overall, and this appears to be due to the external field introducing oscillations to both dipoles which have different phases and can result in ranges of attractive or repulsive interaction.

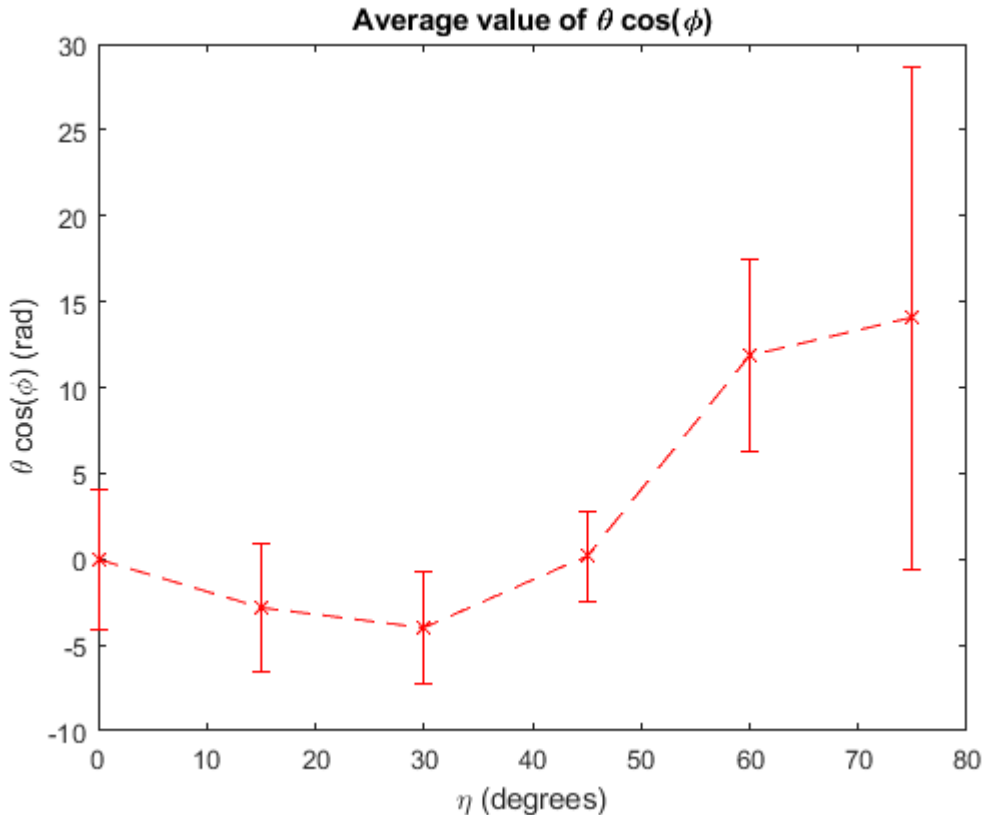


Figure 4.9: In case 3, the average value of $\theta \cos \phi$ shows some of the strange behavior mentioned when discussing the AEPs. The graph first starts to move down, then rises up, but is never more than 15° away from the z axis. The error bars are also relatively constant or slightly decreasing for η less than 50° , which is the barrier where the dipole-dipole force becomes repulsive.

4.4 Fraction of Convergent Paths

Finally, we can look at a graph of the number of paths which reach the blue sphere, as a fraction of the total number of paths at a given η , and track how this fraction varies with η . This graph gives us a direct measure of how likely collision is at a given initial angle. These collections of many dipoles with different initial positions within a certain uncertainty are meant to represent a single wave packet, so this fraction of convergence plot is analogous to a probability of colliding for two quantum mechanical dipoles.

We see that when the dipoles are free to rotate and arbitrarily oriented (the blue line), they have a roughly 80% chance of colliding, which agrees with our intuition. We expect that freely

rotating dipoles can usually align themselves under the influence of their innate fields and attract each other, but in cases where they are extremely misaligned, they don't interact strongly enough to change their orientation before they repel each other. The plot looks essentially flat as η varies.

When an electric field is added in the z direction, the fraction of convergence rises compared to the baseline case 1 at all values of η . This is unintuitive, as we would expect more of the trajectories at large η to diverge when the field points in the z direction. We believe that because the external field classically causes dipoles to oscillate around the field axis, the dipoles at large η spend equal time pointed toward and away from each other, and are thus equally attracted and repelled during their collision. This leads the dominant motion to be simply following their initial path straight toward each other. In the small and intermediate η regions, the dipoles are oscillating entirely within an attractive range of angles, so they feel an overall attraction and bend toward the z axis. Apparently at large η , because the dipoles are so deep in the repulsive regime of their interaction potential, they are hardly attracted toward the north pole at all, but they are still not very much repelled either.

When the dipoles are not allowed to rotate at all, they perfectly follow the dipole-dipole potential discussed in chapter 2. When the force is attractive for the entire trajectory, there is nothing stopping the dipoles from colliding in a nearly perfect head-to-tail alignment. After η crosses into the repulsive regime, some of the dipoles are still able to collide as they enter the attractive regime during their approach, after being moved by the field for some time. When the dipoles are totally misaligned at $\eta = 90^\circ$, there is near zero chance of them ever being attracted close enough for short range physics to have an effect.

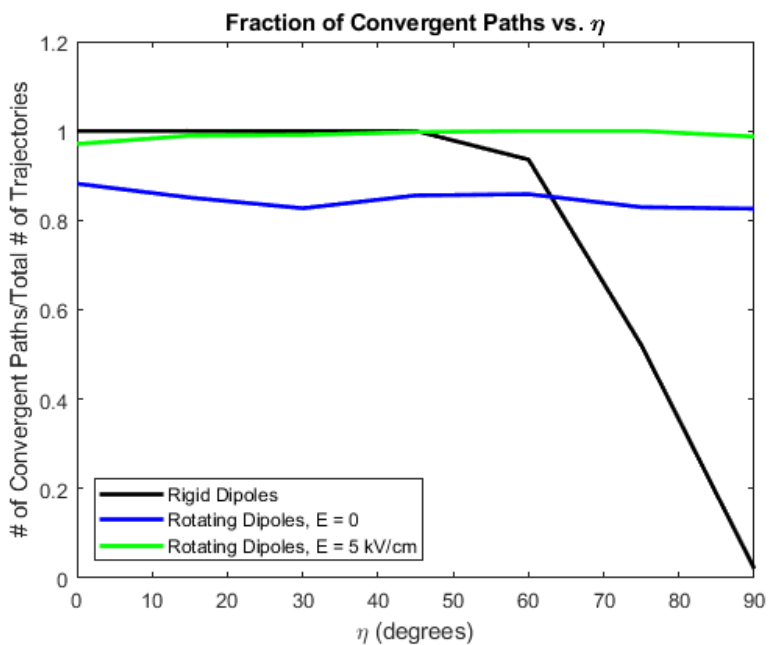


Figure 4.10: Case 1 has a nearly constant fraction of convergence with respect to η . Case 2 stays near unity at all values of η , presumably due to the oscillations of both dipoles. Case 3 has perfect convergence exactly up until the point at $\eta = 55^\circ$ where the dipole-dipole force becomes repulsive. Beyond this point, the fraction of convergence steadily drops.

4.5 Conclusions and Looking Ahead

According to this model, the prospects for control over dipolar molecules before they collide are not quite what we expected. By turning on an electric field, we might increase the likelihood that dipoles collide at a certain angle, but only slightly. An external field of 5 kV/cm also seems to increase the collision rate to nearly unity. This goes against our intuition, but it could be quite a useful property if it translates significantly from the classical picture to experiments. This data implies that as the field is weakened, the fraction of convergence will move down from 1 and eventually meet the $E = 0$ line at about 0.8. If this is correct, then we have a direct way to manipulate what fraction of dipoles collide successfully, although the minimum is quite high. This simulation could be explored at various field strengths and initial temperatures to better flesh out this relationship.

Case 3 seems promising because it looks like the rate of convergence can be adjusted with the angle η . However, this is already not technically a physically achievable scenario, and even if we apply a strong enough electric field to see this control over the probability of colliding manifest, there are other aspects which we seem to have no hope of controlling. In case 3, all of the dipoles which collide do so in a small region centered around the north pole, implying that forcing the dipoles to collide in any orientation other than head-to-tail is not possible when the dipoles are rigidly aligned. This points toward a general lack of control over the dipoles orientation that should be further explored.

This brings me to future goals, of which I have three at the moment: one is to track the final dipole alignment quantitatively in all three cases, another is to vary the external field strength and collect the same data, and the last is to get similar data at even lower initial temperatures.

Tracking the final dipole alignment is the cleanest way to test how our intuition matches with reality. Most physicists probably expect dipoles at ultracold temperatures to automatically align themselves head-to-tail when they collide, especially if no other forces are present. There is some evidence in these plots against that idea already, for the dipoles are sometimes repelling each other even when they approach along the axis of an external field helping them align. Exploring the dipole alignment fully will tell us if we are overestimating the potency of the dipole-dipole interaction.

Varying the field strength should help quantify the relationship between E and the convergence fraction, and it will also raise our confidence in this result if we see similar phenomena at different magnitudes of E . Finding a mathematical relationship between the collision rate and the strength of the external field would give us a result that could be conclusively tested in experiment.

Regarding more data, I should preface by saying that all of the simulations and calculations done for this thesis were done on my personal laptop, which I bought for the purpose of playing video games. I believe that my device performed admirably and created some useful data, but I also believe that a more powerful machine could easily calculate the same trajectories at μK or even nK scales. This is important to our understanding because the collision energy being high

suppresses all other changes to the motion, and if experimental techniques continue to improve, there could be a lower temperature range where much more control is possible.

In summary, we have found that our intuitions regarding long range interactions of dipolar molecules, at least on the temperature scale of mK, are quite off. The tendency of dipoles to align themselves head-to-tail is frequently disrupted by molecular rotations, and the effects of an external field, at least classically, are very strange due to the dipoles' oscillations. More data gathered at lower temperature scales and different field strengths along with analysis of how the final dipoles are aligned would allow us to draw stronger conclusions about what experiments can do to change how dipolar molecules interact.

Bibliography

- [1] D. J. Wineland, R. E. Drullinger, and F. L. Walls. Radiation-pressure cooling of bound resonant absorbers. Phys. Rev. Lett., 40:1639–1642, Jun 1978.
- [2] S. Ospelkaus, K.-K. Ni, D. Wang, M. H. G. de Miranda, B. Neyenhuis, G. Quéméner, P. S. Julienne, J. L. Bohn, D. S. Jin, and J. Ye. Quantum-state controlled chemical reactions of ultracold potassium-rubidium molecules. Science, 327(5967):853–857, 2010.
- [3] Hidetoshi Katori, Masao Takamoto, V. G. Pal’chikov, and V. D. Ovsiannikov. Ultrastable optical clock with neutral atoms in an engineered light shift trap. Phys. Rev. Lett., 91:173005, Oct 2003.
- [4] C. Monroe, W. C. Campbell, L.-M. Duan, Z.-X. Gong, A. V. Gorshkov, P. W. Hess, R. Islam, K. Kim, N. M. Linke, G. Pagano, P. Richerme, C. Senko, and N. Y. Yao. Programmable quantum simulations of spin systems with trapped ions. Rev. Mod. Phys., 93:025001, Apr 2021.
- [5] M.-G. Hu, Y. Liu, D. D. Grimes, Y.-W. Lin, A. H. Gheorghe, R. Vexiau, N. Bouloufa-Maafa, O. Dulieu, T. Rosenband, and K.-K. Ni. Direct observation of bimolecular reactions of ultracold krb molecules. Science, 366(6469):1111–1115, 2019.
- [6] David J. Griffiths. Introduction to electrodynamics. Cambridge University Press, 4th edition, 2018.
- [7] Lawrence W. Cheuk, Loïc Anderegg, Yicheng Bao, Sean Burchesky, Scarlett S. Yu, Wolfgang Ketterle, Kang-Kuen Ni, and John M. Doyle. Observation of collisions between two ultracold ground-state caf molecules. Phys. Rev. Lett., 125:043401, Jul 2020.
- [8] Svetlana Kotochigova. Dispersion interactions and reactive collisions of ultracold polar molecules. New Journal of Physics, 12:073041, 2010.